Influence of Electrode Height on Carbon Nanotube Electrochemical Biosensors

Benjamin J. Brownlee and Brian D. Iverson
Department of Mechanical Engineering
Brigham Young University

ABSTRACT

High sensitivity of electrochemical sensors enables the detection of low concentrations of target analyte. Being able to quickly and accurately detect low concentrations of proteins at point-of-care allows for results to be analyzed more easily and effectively. Having high surface area allows for more analyte to be detected, possibly leading to increased sensitivity. Vertically-aligned carbon nanotubes (VACNTs) were patterned into interdigitated electrodes (IDEs) and then functionalized with the representative protein streptavidin to demonstrate sensing of biotin. Three electrode heights were investigated to determine the influence of electrode height on sensor sensitivity. Cyclic voltammetry and electrochemical impedance spectroscopy were used to characterize the electrodes and track the associated changes with the addition of streptavidin and biotin. A change in imaginary impedance at 147 Hz was shown to have the largest sensitivity. Height was shown to have a significant impact on sensor response, particularly at higher concentrations, with 80 µm tall VACNTs having 138% change in impedance when adding streptavidin and biotin.

INTRODUCTION

Point-of-care diagnostics has gained interest among researchers because it enables cost effective and rapid results that were typically done by enzyme-linked immunosorbent assays (ELISA), a process that requires extensive equipment and expertise and longer processing times. Development of electrochemical biosensors have pushed toward the ability diagnose at point-of-care use. While other methods of detection have been used, such as optical methods, electrochemical sensors have the advantage of being repeatable, affordable, and easy to use [1]. In particular, electrochemical sensors that are in an interdigitated electrode (IDE, see Figure 1A) design exhibit low ohmic drops, high signal-to-noise ratios, and fast response times [2].

Carbon nanomaterials (carbon nanotubes, graphene, and graphene oxide), have been shown to be effective at increasing sensor sensitivity [3]. Specifically, microstructured surfaces, greatly increase electrode surface area and have been shown to outperform planar geometries [4]. Vertically-aligned carbon nanotubes (VACNTs) are an excellent example as they provide high surface area to volume ratio and are highly conductive, making VACNTs a useful electrochemical electrode nanomaterial.

VACNTs have previously been used in an IDE configuration for the detection of an oral cancer markers [5] and this work seeks to build upon and generalize the findings that work. VACNTs have also been used for detection of hydrogen peroxide (H_2O_2) with a flow-through VACNT electrode [6]. The three dimensional nature of the VACNT electrode, as schematically shown in Figure 1B, provides the advantage of having a large surface-area-to-volume ratio that enables higher protein capture capacity relative to planar electrodes, leading to improved sensitivity [7].

In the present work we have fabricated VACNT IDEs at heights of 5, 20 and 80 µm for impedance-based biosensing. The electrodes were functionalized by covalently binding the representative protein streptavidin on to the VACNT surfaces. Biotin was then bound to the streptavidin as an example of small molecule detection. Cyclic voltammetry and electrochemical impedance spectroscopy were used to characterize the electrodes and track the associated changes with the addition of streptavidin and biotin. A change in imaginary impedance was shown to have the largest sensitivity. Height was shown to have a significant impact on sensor response, particularly at higher concentrations.

MATERIALS AND METHODS

The IDE design is illustrated in Figure 1A, where dark red and blue areas (central region) represent patterned forests of VACNTs acting as the electrodes and light red and blue areas (left and right edges) represent thin chromium (Cr) electrical leads underneath an aluminum oxide (Al_2O_3) layer. Figure 1B illustrates the three-dimensional nature of VACNT IDE electrodes.

The electrode length (L) was 2.95 mm, the electrode width (w_e) was 25 µm, and the gap width (w_g) was 25 µm. Three VACNT heights (h) of the IDE electrode arrangement were compared (5, 25, and 80 µm). Each IDE sensor had 61 total fingers (30 and 31 per side), with a total electrode area of 4.5 mm^2. The two Cr electrical leads for each sensor are 13 mm x 0.5 mm.

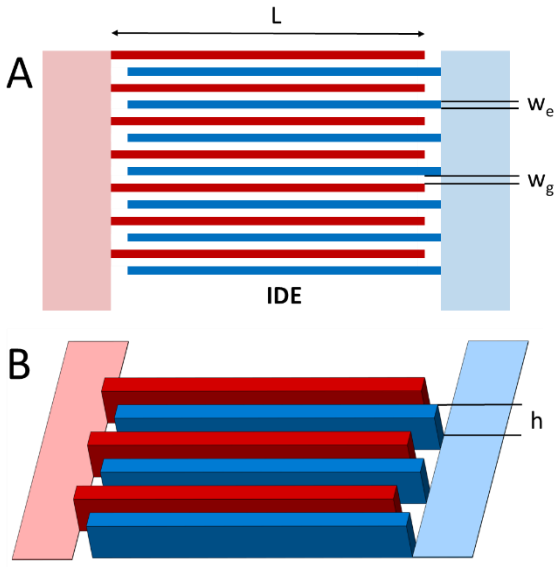

Figure 1. (A) Schematic of IDE electrode arrangement with electrode length (L), electrode width (w_e), and gap width (w_g) represented. Dark colors represent regions of VACNTs and light colors represent Cr leads. (B) Schematic emphasizing 3D nature of VACNT IDE electrodes with electrode height (h) represented.

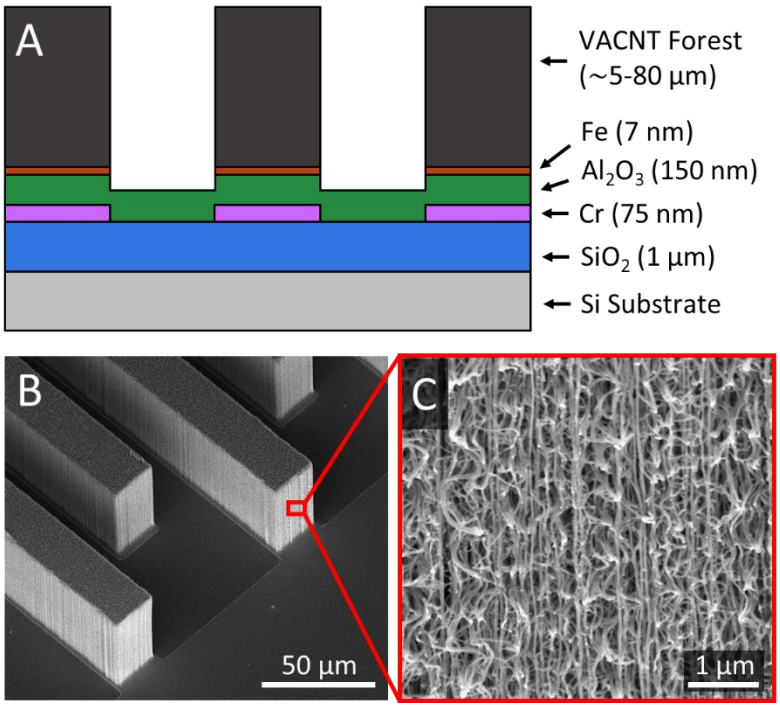

Figure 2. (A) Schematic of layers used to fabricate the VACNT sensor architecture: Si, SiO_2, Cr, Al_2O_3, Fe, and VACNTs. Scanning electron microscope (SEM) images of (B) 3D VACNT electrodes and (C) magnified VACNTs, showing porous nature of electrode

Photolithography was used to pattern positive photoresist (AZ3330) on a 100 mm diameter, oxidized silicon (Si) wafer (1 µm thick oxide, see Figure 2A for processing). Patterned photoresist was used to create the electrode designs from Figure 1 and the Cr electrical leads for each electrode (13 mm x 0.5 mm). A 75 nm layer of Cr was deposited onto the patterned photoresist by e-beam evaporation. A lift-off process was performed by sonication in N-methyl-2-pyrrolidone (NMP) for 30 min, leaving only patterned Cr on the oxidized wafer. In this manner, Cr was deposited below all 3D electrode regions and as electrical leads to the sensor electrodes. After covering the contact pads to the electrical leads with permanent marker, 150 nm of aluminum oxide (Al_2O_3) was deposited by e-beam evaporation. NMP sonication was performed for 5 min to expose the contact pads by removing the marker ink and Al_2O_3 for electrical connects. Planar, Cr electrical leads underneath Al_2O_3 can be seen in Figure 2B as the lighter region on the substrate. A second photolithography process was used to cover the wafer in photoresist except in regions where sensor fingers are to be constructed. A 7 nm film of iron (Fe) was thermally evaporated onto the patterned photoresist, followed by sonication in NMP for 15 minutes leaving patterned Fe on a portion of the Al_2O_3/Cr layer. In this manner, the catalyst for CNT growth was patterned so that growth would only occur in the 3D electrode regions. The patterned wafer was diced into 16.1 mm x 8 mm rectangles using a dicing saw with a diamond-coated blade.

VACNT growth methods were similar to previously published protocols [6, 8]. VACNTs were grown by chemical vapor deposition (CVD) in a 1-inch diameter Lindberg/Blue M tube furnace with flowing hydrogen (H_2, 311 sccm) and ethylene (C_2H_4, 338 sccm) at 750 °C for 5, 30, or 120 s. The temperature was then raised to 900 °C and the C_2H_4 flow rate reduced to 193 sccm to infiltrate (coat) the VACNTs with amorphous carbon for 60 s. This infiltration process strengthened the VACNTs to create mechanically sturdy, porous microstructures (see Figure 2B and C). The electrodes were oxygen plasma etched (250 W, 300 mTorr, 30 – 60 s) until the two electrodes were electrically isolated using a Technics Planar Etch II machine.

Carbon-coated VACNTs are slightly hydrophobic after they are grown. An oxygen plasma etch was used to remove the amorphous carbon

in between electrodes and also served to change the VACNTs from hydrophobic to hydrophilic [8]. This hydrophilicity is important to ensure that the solution is wetting the entire electrode and to promote close contact between the molecules in solution and the electrode surface.

All electrochemical experiments were performed with a CH Instruments (CHI) 660E Potentiostat/ Galvanostat in a two-electrode configuration where one VACNT electrode was the working electrode and the other VACNT electrode was the counter/reference electrode. The Cr contact pads were contacted by micro-manipulation probes. The electrolyte was a static 50 µL droplet of 5 mM potassium ferricyanide ($K_3[Fe(CN)_6]$), 5 mM potassium ferrocyanide ($K_4[Fe(CN)_6]$), and 100 mM KCl in phosphate buffered saline (PBS, 1X, pH 7.4, Fisher Scientific). Cyclic voltammetry (CV) was performed between -600 mV and 600 mV relative to the VACNT electrode at scan rates of 150 mV/s to 1250 mV/s. Ohmic drop correction was used to account for the resistance within the Cr electrical leads (about 300 Ω). The frequencies for electrochemical impedance spectroscopy (EIS) ranged from 10,000 Hz to 0.1 Hz, with an input amplitude of 10 mV.

The VACNT electrodes were incubated in a 50 µL droplet of 100 mM EDC and 100 mM NHS in 0.1 M 2-(N-morpholino) ethanesulfonic acid (MES, pH 4.7, Thermo Scientific 28390) for 60 min. The VACNT electrodes were then rinsed and soaked in PBS for 20 min. A 20 µL droplet of 500 µg/mL, fluorescently tagged Atto 425 streptavidin (F-SA, Sigma Aldrich 09260) in PBS was placed on the EDC/NHS-activated VACNTs for 60 min to bind the SA protein to the VACNTs (Figure 3). Electrodes were then rinsed and allowed to soak in PBS for 40 min. While the stock F-SA solution was stored at 4 °C, all functionalization steps and soakings were performed at room temperature.

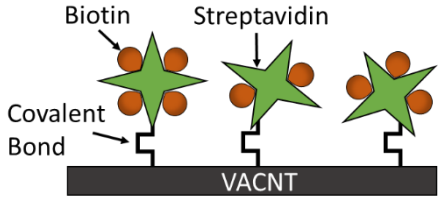

Figure 3. Schematic of functionalized VACNTs showing the larger streptavidin covalently bound to the VACNT surface and the smaller biotin bound with the streptavidin.

A 20 µL droplet of 1 ng/mL fluorescently tagged Atto 565 biotin (F-biotin, Sigma-Aldrich 92637) in PBS was placed on F-SA/VACNT sensors for 20 min, which binds to the F-SA as depicted in Figure 3. The sensor was then rinsed and allowed to soak in 50 µL of PBS for 1 minute, after which electrochemical measurements were taken. The concentration of F-biotin was incrementally increased for each measurement following the same procedure above for each concentration (0.01, 0.1, 1, 10, and 100 µg/mL).

RESULTS AND DISCUSSION

VACNT electrode heights were measured using optical profilometry. CVD growth times of 5, 30, and 120 s corresponded with approximately 5, 20, and 80 µm electrode heights, respectively. With the spacing and width of the IDEs being 25 µm, the height-to-width ratio of the electrodes ranged from 0.2 to 3.2.

Cyclic voltammetry (CV) was performed to characterize the VACNT IDEs. By sweeping the applied potential, CV can give important information about the geometry and electroactivity of an electrode. Figure 4A shows cyclic voltammograms of VACNT electrodes of varying heights (5, 20, and 80 µm) at a constant scan rate of 1000 mV/s in a static 50 µL droplet of ferricyanide solution. The overall shape of the curves is typical for the single electron electrochemical reaction involving ferricyanide, having anodic and cathodic peaks in current. The peaks are caused by a balance between reaction kinetics and diffusion from the solution and are symmetric about 0 V because the reference is to a VACNT electrode and not a dedicated reference electrode such as Ag/AgCl.

Figure 4A shows that VACNT height causes a significant difference in the peak current, with the 80 µm peak current being about 7.2x greater than the 5 µm. The electroactive surface area of an electrode is linearly proportional to the peak current (i_p) as given by the Randles-Sevcik equation at 25 °C:

$$i_p = (2.69\text{x}10^5)n^{3/2}AD^{1/2}Cv^{1/2}$$

where n is the number of electrons transferred (n=1), A is the electroactive area of the electrode (units of cm^2), D is the diffusion coefficient of ferricyanide ($7.2\text{x}10^{-6}$ cm^2/s), C is the ferricyanide concentration (5 mM or $5\text{x}10^{-6}$ mol/cm^3), and ν is the scan rate (0.125 to 1.25 V/s). The only variable that is not well defined is the electrode surface area. The 2D geometric area of the electrode pattern is known to be 0.022 cm^2 ($30Lw_e$), but the exact surface area of the electrode is not known because of the porous nature of the VACNTs. The calculated electroactive surface areas for the 80, 20, and 5 µm tall VACNTs were 0.33, 0.13, and 0.046 cm^2, respectively. Thus, the electroactive surface area of the 80 µm tall electrode was 15x larger than the 2D geometric area, with the actual surface area likely being even higher because of the electrode porosity.

The peak current increased with scan rate, as can be seen in Figure 4B for 80 µm tall VACNTs. It is

interesting to note that the shape of the CV curve transitions from prominent peaks at high scan rates to a more sigmoidal shape with no peak at the lowest scan rate. This occurs because the electrodes are close enough together to cause a diffusion limited scenario at slower scan rates, typical of microelectrode arrays. The peak-to-peak potential separation was about 85 mV, which is close to the theoretical peak separation of 59 mV. According to Equation 1, the peak current should be linearly proportional to the square root of scan rate, which is plotted in Figure 4C for the three different VACNT heights. This linearity confirms that the VACNT electrode and the electrochemical reaction indicate reversible behavior.

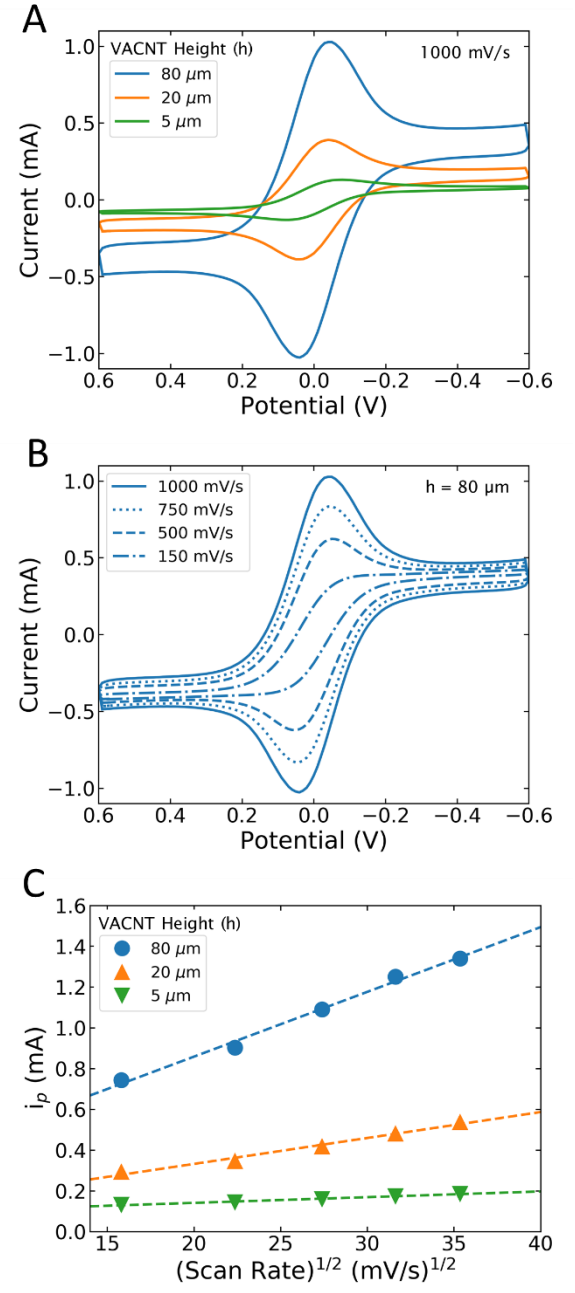

Figure 5. Cyclic voltammograms of VACNT electrodes in ferricyanide solution. (A) 80, 20, and 5 μm tall VACNT IDEs at a scan rate of 1000 mV/s. (B) 80 μm tall VACNT IDE at scan rates of 1000, 750, 500, and 150 mV/s. (C) Peak current i_p with the square root of scan rate for 80, 20, and 5 μm tall VACNTs.

Electrochemical impedance spectroscopy (EIS) was performed by applying a sinusoidal potential to the electrode and measuring the corresponding current to obtain an impedance over a wide range of frequencies. Nyquist plots are a convenient way to show the results from EIS, where imaginary impedance (-Z") is plotted with respect to real impedance (Z') over a range of frequencies. Nyquist plots for 80, 20, and 5 μm tall IDEs are shown in Figure 5, where the impact of VACNT height on the baseline EIS measurement is evident by the change in magnitude of the semi-circular curves. The impedance was much larger for the 5 μm tall VACNTs than for the 80 μm tall VACNTs, an observation that correlates well with the larger current observed from the CV data (Figure 4) as a result of the higher surface area. Smaller semi-circles were also observed at the base of the large semi-circles and followed the same trend as the larger semi-circles. The data markers in the Nyquist plots in Figure 5 are the measured experimental EIS results for VACNT IDEs taken after EDC/NHS chemical activation but before the addition of streptavidin or biotin.

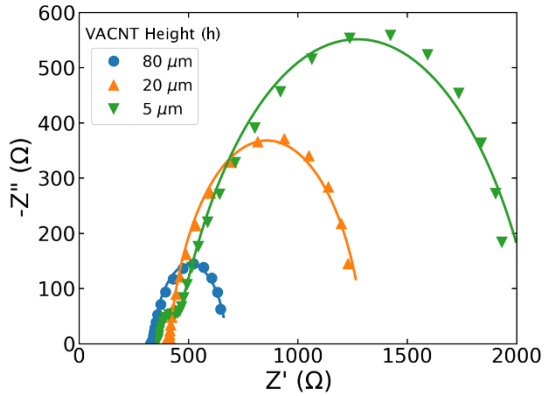

Figure 4. Experimental (markers) and simulated (lines) Nyquist plots of 80, 20, and 5 μm tall VACNT IDEs with no streptavidin/biotin.

The impedance change associated with F-SA and F-biotin binding to a sample sensor surface is shown in Figure 6A and B for an 80 μm tall VACNT IDE. As shown in Figure 6A, there was a slight change observed in the resistance of the diffusion-driven large semi-circles when adding F-SA and F-biotin to the VACNTs (1.8% F-SA, 3.5% F-SA+F-biotin), but there was a much larger change observed in the resistance of the kinetics-driven small semi-circles shown in Figure 6B (32% F-SA, 138% F-SA+F-biotin). Thus, it is

advantageous to focus on the changes that occur at the higher frequencies associated with the kinetics at the electrode surface.

The imaginary component of impedance (Z") exhibited the largest relative change when F-biotin was bound to the VACNTs. Figure 6C shows the relative change in imaginary impedance at 147 Hz for 80, 20, and 5 µm tall VACNTs for different concentrations of F-biotin, where the percent change is measured relative to the imaginary impedance at 147 Hz after functionalizing with F-SA. The percent change in imaginary impedance was calculated across all measured frequencies and it was determined that 147 Hz gave the highest signal for all heights. The location of the 147 Hz impedance is on the right side of the small semi-circle, as shown by the data markers outlined in black in Figure 6B. As opposed to tracking the change in imaginary impedance, the EIS data can also be curve fit to an equivalent circuit model with circuit elements that would change in response to changes in the shape of the Nyquist plot. It was found that the relative change in imaginary impedance generally gave a higher signal than the change in curve fit resistance. The data in Figure 6C represents the average of three sensors, with the error bars indicating the standard deviation.

In Figure 6C it can be seen that the changes in impedance were small at lower concentrations of F-biotin (1 ng/mL to 1 µg/mL), and then there was a sudden spike in impedance at 10 µg/mL F-biotin, potentially leading to two linear sensing regions. While the exact cause of this phenomenon is unknown, it is possible that higher concentrations of F-biotin allow the molecules to better penetrate the porous VACNT electrode because of a higher concentration gradient, thus utilizing more of the surface area in between VACNTs. The 80 µm VACNTs provided an average change of 7% from 0.001 – 1 µg/mL F-biotin and an average change of 95% from 1 – 100 µg/mL F-biotin, with an overall maximum change of 107% relative to F-SA at 100 µg/mL F-biotin. The tall VACNTs (80 µm) generally demonstrated a larger relative change in impedance with F-SA and F-biotin, likely due to the additional surface area compared to the shorter electrodes and because the baseline impedance of the bare VACNTs was the smallest.

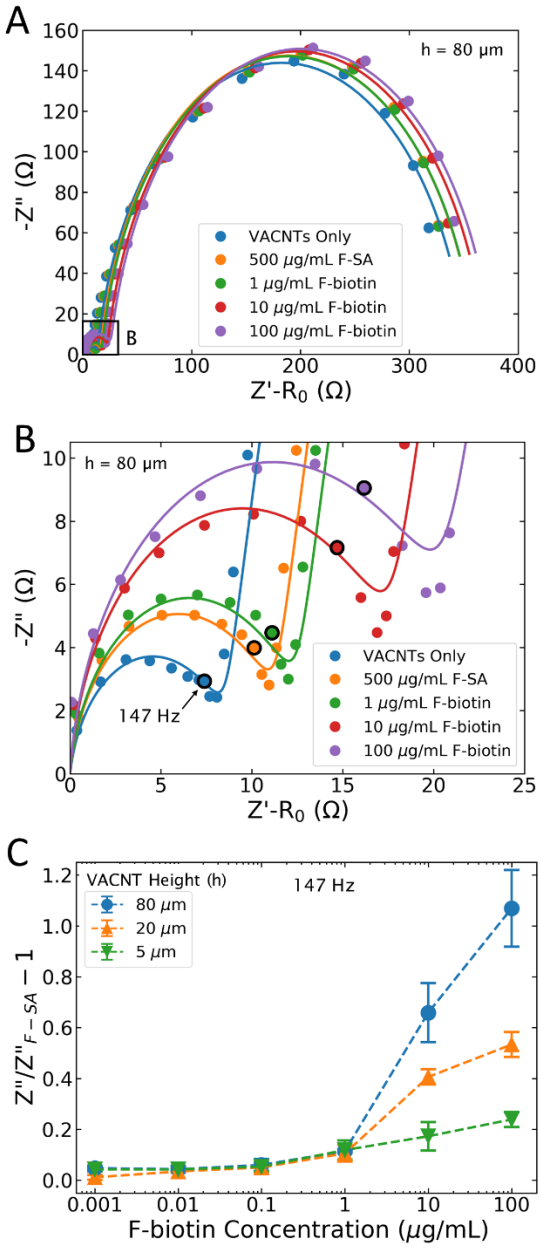

Figure 6. (A) 80 µm tall VACNT IDEs with subsequent addition of 500 µg/mL F-SA and 1, 10, and 100 µg/mL F-biotin. (B) Zoomed in view of the first semi-circle, with 147 Hz marked with a black outline. (C) Relative change in imaginary impedance at 147 Hz as function of F-biotin concentration for 80, 20, and 5 µm tall VACNT IDEs. The error bars represent the standard deviation for three different sensors.

CONCLUSION

This work has characterized porous, 3D VACNTs electrodes for impedance-based biosensing. Electrode height was shown to have a large impact on CV and EIS curves, with tall 80 µm VACNTs having the highest calculated electroactive surface area at 15x the 2D geometric area. The VACNT IDEs have been shown to be effective biosensors by taking advantage of high surface area provided by 3D VACNT electrode structure. A change in imaginary impedance at 147 Hz was shown to have the largest sensitivity, with 80 µm tall VACNTs having up to 138% change in impedance when adding streptavidin and biotin. The change in impedance for the representative target analyte bound to the VACNT electrode surface could be used to detect a large range of target analyte depending on what is

functionalized to the VACNT surface. Thus, future work could involve the detection of other target analyte.

REFERENCES

[1] S.A. Zaidi, J.H. Shin, Recent Developments in Nanostructure Based Electrochemical Glucose Sensors, Talanta 149 (2016) 30-42.

[2] M. Varshney, Y. Li, B. Srinivasan, S. Tung, A label-free, microfluidics and interdigitated array microelectrode-based impedance biosensor in combination with nanoparticles immunoseparation for detection of Escherichia coli O157:H7 in food samples, Sensors and Actuators B: Chemical 128(1) (2007) 99-107.

[3] K. Dhara, D.R. Mahapatra, Electrochemical Nonenzymatic Sensing of Glucose Using Advanced Nanomaterials, Microchimica Acta 185(1) (2018) 49.

[4] F. Schröper, D. Brüggemann, Y. Mourzina, B. Wolfrum, A. Offenhäusser, D. Mayer, Analyzing the electroactive surface of gold nanopillars by electrochemical methods for electrode miniaturization, Electrochimica Acta 53(21) (2008) 6265-6272.

[5] S. Ding, S.R. Das, B.J. Brownlee, K. Parate, T.M. Davis, L.R. Stromberg, E.K.L. Chan, J. Katz, B.D. Iverson, J.C. Claussen, CIP2A Immunosensor Comprised of Vertically-aligned Carbon Nanotube Interdigitated Electrodes Towards Point-of-Care Oral Cancer Screening, Biosensors and Bioelectronics 117 (2018) 68-74.

[6] B.J. Brownlee, K.M. Marr, J.C. Claussen, B.D. Iverson, Improving Sensitivity of Electrochemical Sensors with Convective Transport in Free-standing, Carbon Nanotube Structures, Sensors and Actuators B: Chemical 246 (2017) 20-28.

[7] D. Kim, A.E. Herr, Protein immobilization techniques for microfluidic assays, Biomicrofluidics 7(4) (2013) 041501.

[8] K.M. Marr, B. Chen, E.J. Mootz, J. Geder, M. Pruessner, B.J. Melde, R.R. Vanfleet, I.L. Medintz, B.D. Iverson, J.C. Claussen, High Aspect Ratio Carbon Nanotube Membranes Decorated with Pt Nanoparticle Urchins for Micro Underwater Vehicle Propulsion via H2O2 Decomposition, ACS Nano 9(8) (2015) 7791-7803.